Modular ellipsometric approach for mining structural information from nonlinear optical polarization analysis

Ryan M. Plocinik, R. Michael Everly, Andrew J. Moad, and Garth J. Simpson*
Department of Chemistry, Purdue University, 560 Oval Drive, West Lafayette, Indiana 47907
(Received 8 February 2005; revised manuscript received 13 May 2005; published 7 September 2005)

An ellipsometric approach is described for interpreting polarization information in surface second harmonic generation (SHG). The general applicability of nonlinear optical ellipsometry (NOE) was demonstrated in SHG measurements of uniaxial films under resonant, near-resonant, and nonresonant conditions. The modularity inherent in the instrumental design allows the same basic mathematical formalism to be used to describe a diverse array of optical configurations for polarization analysis. This methodology is particularly useful in spectroscopic and resonance-enhanced SHG and SFG measurements, in which intensity-based methods are generally not applicable. In one application, SHG polarization measurements were used for what is believed to be the first time to measure ratios of the dominant elements of the tensor describing two-photon absorption.

DOI: 10.1103/PhysRevB.72.125409 PACS number(s): 78.68.+m, 42.65.Ky, 07.60.Fs

I. INTRODUCTION

Second harmonic generation (SHG) and sum-frequency generation (SFG) have emerged as powerful probes for characterizing oriented surfaces and interfaces. In surface measurements, the signals for both SHG and SFG measurements arise predominantly from oriented chromophores at the interface, as the phenomena are electric-dipole forbidden in random media. Surface-specific spectroscopic measurements have exploited this symmetry condition to probe solid/liquid,[1–5] liquid/liquid,[1,2,4,6–10] liquid/air,[1–3,5–8,10–13] solid/air,[2,12,14] semiconductor,[1,10,11,13,15,16] polymer,[17] and biological[11,12] interfaces.

In the limit of identical noninteracting chromophores, the molecular nonlinear polarizability is related to the surface $\boldsymbol{\chi}^{(2)}$ tensor elements through Eq. (1), where N_s is the surface number density of the chromophore and $R_{\Lambda\lambda}$ is the element of the Euler transformation matrix relating the molecular coordinate λ to the surface (laboratory) coordinate Λ:

$$\chi_{IJK} = N_s \langle R_{Ii'} R_{Jj'} R_{Kk'} \rangle \beta_{i'j'k'}. \tag{1}$$

For SHG in uniaxial systems, all but 4 of the 27 possible surface $\boldsymbol{\chi}^{(2)}$ tensor elements are either zero or can be expressed in terms of other tensor elements, leaving only χ_{ZZZ}, $\chi_{ZXX}=\chi_{ZYY}$, $\chi_{XXZ}=\chi_{XZX}=\chi_{YYZ}=\chi_{YZY}$, and $\chi_{XYZ}=\chi_{XZY}=-\chi_{YXZ}=-\chi_{YZX}$ remaining. If the uniaxial system is achiral, χ_{XYZ} disappears as well.

Under most experimental conditions, the molecular polarizability tensor $\boldsymbol{\beta}^{(2)}$ in Eq. (1) can be expressed in terms of simple, intuitive molecular properties. In SFG and SHG measurements in which an *incident* frequency is resonant with a real transition within the surface chromophore, including vibrational SFG investigations, the resonant molecular nonlinear polarizability simplifies to the product of the transition moment and the anti-Stokes Raman polarizability tensor [shown in Eq. (2) for ir-vis SFG, with the underscore indicating the resonant interaction]:[18,19]

$$\beta_{i'j'k'}(-\omega_{\text{sum}};\omega_{\text{vis}},\underline{\omega_{ir}}) = \frac{-1}{2\hbar}\sum_n \frac{(\alpha_{0n}^{i'j'})_{AR}\mu_{n0}^{k'}}{(\omega_n - \omega_{\text{ir}} - i\Gamma_n)}. \tag{2}$$

Under conditions in which the states dominating the molecular nonlinear optical response lie near or higher in energy than the sum frequency, including most SHG measurements, the nonlinear polarizability of the chromophore simplifies to the product of the transition moment and the tensor for two-photon absorption (TPA), shown in Eq. (3)[19]

$$\beta_{i'j'k'}(\underline{-2\omega};\omega,\omega) = \frac{-1}{2\hbar}\sum_n \frac{\mu_{0n}^{i'}(\alpha_{n0}^{j'k'})_{\text{TPA}}}{(\omega_n - 2\omega - i\Gamma_n)}. \tag{3}$$

The additional factor of 2! arising from the degeneracy in the incident frequency in SHG is implicitly included in the definition of the TPA tensor. Using the relations in Eqs. (1), (2), and (3), reliable measurements of the macroscopic nonlinear polarizability described by the $\boldsymbol{\chi}^{(2)}$ tensor elements can provide rich information about both molecular orientation and the nonlinear polarizability of the chromophore. Polarization analysis in SHG and SFG has traditionally been performed by separately recording the intensities of the *p*- and *s*-polarization components of the exigent beam as functions of the incident polarization(s).

Despite their ubiquitous use, intensity-based approaches can be problematic in polarization analysis. In general, the $\boldsymbol{\chi}^{(2)}$ tensor elements become complex valued at or near resonance. The numerous cross terms introduced between the various real and imaginary values complicates rigorous extraction of the $\boldsymbol{\chi}^{(2)}$ tensor elements in most spectroscopic applications. In brief, there are often more unknowns than equations under these conditions.[20] Even under the best of circumstances, most simple intensity-based analysis methods only yield the relative magnitudes of the $\boldsymbol{\chi}^{(2)}$ tensor elements and contain little or no relative sign or phase information.

One particularly illustrative example of the importance of phase information in nonlinear optical polarization measurements arises in studies of chiral systems. Several experimental methods have been developed for probing the large chiral

effects routinely observed in SHG and SFG measurements of thin surface layers.[21–34] For example, SHG circular dichroism (CD) is a measurement of the intensity difference detected for left (L) vs right (R) circularly polarized incident light. In related measurements, SHG linear dichroism (LD) is the difference between SHG intensities generated for plane polarized light with the axis of polarization oriented $-45°$ and $+45°$.[21–23,35–38] The relationships between the measured SHG-CD and SHG-LD ratios and the surface tensor elements are summarized below[24,35,36,39,40]

$$R_i^{\mathrm{CD}} = \frac{I_{i,L}^{2\omega} - I_{i,R}^{2\omega}}{\frac{1}{2}\left(I_{i,L}^{2\omega} + I_{i,R}^{2\omega}\right)} = 4\frac{\mathrm{Im}(2\chi_{isp}\chi_{ipp}^{*})}{|2\chi_{isp}|^2 + |\chi_{ipp}|^2}, \tag{4}$$

$$R_i^{\mathrm{LD}} = \frac{I_{i,-45°}^{2\omega} - I_{i,45°}^{2\omega}}{\frac{1}{2}\left(I_{i,-45°}^{2\omega} + I_{i,45°}^{2\omega}\right)} = 4\frac{\mathrm{Re}(2\chi_{isp}\chi_{ipp}^{*})}{|2\chi_{isp}|^2 + |\chi_{ipp}|^2}. \tag{5}$$

In Eqs. (4) and (5), $I^{2\omega}$ is the detected intensity of the frequency doubled beam, with the subscripts indicating the detected polarization component i (either s or p) generated for a given incident polarization state, and Jones tensor elements are used, which are linear combinations of the surface tensor elements and geometric and Fresnel factors relating the incident and exigent electric fields to the fields within the interfacial layer (explicit expressions for the Jones tensor elements are given later in the text). SHG optical rotary dispersion (ORD), in which chiral contributions result in rotation of the primary polarization axis of the exigent beam, is closely related to both SHG-CD and SHG-LD. In SHG-ORD measurements, a polarizer is placed between the sample and the detector and the intensity is recorded as a function of the polarizer rotation angle. Fitting the detected SHG intensity to the following expression yields the SHG-ORD rotation angle ϕ:[37,38,41–43]

$$I^{2\omega} = F + G\cos^2(\alpha_{\mathrm{pol}} - \phi). \tag{6}$$

SHG-ORD measurements are typically performed with a p-polarized incident beam to simplify their interpretation, in which case ϕ_p is zero in the absence of surface chirality in uniaxially oriented films.[37,38,41–43] Clearly, in SHG-CD, SHG-LD, and SHG-ORD measurements of interfacial chirality, the relative phase shifts between the Jones tensor elements are critical aspects of all of the measured parameters, but this phase information is generally unavailable using most existing intensity-based polarization analysis techniques.

In previous work, a null ellipsometric analysis approach was developed for acquiring and interpreting polarization measurements in SHG surface investigations.[20] In the present study, the mathematical framework describing nonlinear optical ellipsometry was generalized to be compatible with a host of different optical configurations and ellipsometric characterization approaches. Specifically, nonlinear optical null ellipsometry (NONE), rotating analyzer ellipsometry (RAE), and rotating quarter wave plate ellipsometry (RQE) in SHG can all be understood using a single compact set of modular mathematical expressions (Fig. 1). In NONE, a quarter wave plate is combined with either a rotating polarizer or a combination of a rotating half wave plate and a fixed polarizer, and the rotation angles producing a minimum in the detected intensity are used to determine the complete polarization state. In RAE, the intensity of the beam is recorded as a function of the rotation angle of a polarizer, and analysis of the resulting detected response yields the polarization state of the beam. RQE is conceptually similar to RAE, except the polarized intensity as a function of a quarter wave plate rotation angle is used to determine the polarization state rather than the polarizer rotation angle. Combining ellipsometry measurements obtained for linearly and circularly polarized incident polarizations allows determination of the full set of complex-valued $\boldsymbol{\chi}^{(2)}$ tensor elements with retention of relative phase and amplitude information in both chiral and achiral uniaxially oriented films. In addition, ellipsometric measurements in SHG are shown to yield information on the polarization dependence of two-photon absorption.

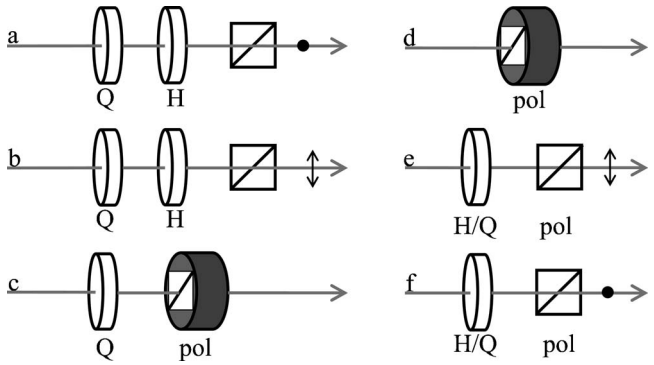

FIG. 1. Configurations for the detection optical pathway (arrow represents the direction of the laser beam) where (a) has two rotating wave plates and a polarizer set to pass s-polarized light; (b) has two rotating wave plates and a polarizer set to pass p-polarizer light; (c) has a rotating quarter-wave plate and rotating polarizer; (d) has a rotating polarizer; (e) has a rotating wave plate and polarizer set to pass p; and (f) has a rotating wave plate and polarizer set to pass s.

II. THEORY

A modular approach in the NOE instrument allows multiple experimental configurations to be understood within a single compact and intuitive mathematical framework. The three modules of the instrument consist of (1) the optics between the sample and the detector, (2) the sample configuration, and (3) the optics used to prepare the polarization state of the incident beam. The inherent flexibility of the ellipsometric analysis approach allows for a large degree of interchangeability between the optical configurations in each module. It is convenient to start with the optics following the sample.

A. Measuring the complete polarization state of the nonlinear optical beam

A diverse array of methods has been developed previously for traditional linear ellipsometry analyses. Several of the

most common approaches (depicted in Fig. 1) can be directly adapted for nonlinear optical ellipsometry. Three different null-ellipsometric configurations for extracting the complete polarization state are considered. In the first [Fig. 1(a)], the nonlinear beam generated at the interface is passed through a quarter wave plate (Q), a half wave plate (H), and a polarizer set to pass s-polarized light. The second optical pathway is identical to the first except the polarizer is set to pass p-polarized light [Fig. 1(b)]. In the third, a quarter wave plate and a rotating polarizer are employed [Fig. 1(c)]. In addition, ellipsometry can be performed by Fourier analysis of the detected intensity using either a rotating analyzer [Fig. 1(d)], a rotating half-wave plate [Figs. 1(e) and 1(f)], or a rotating quarter wave plate [Figs. 1(e) and 1(f)].

For both SHG and SFG, the optical components used for detecting the polarization state of the nonlinear beam depicted in Fig. 1 can be treated using a series of Jones matrices.[44] The Jones matrix for a polarizer (pol) rotated an arbitrary angle γ with respect to the p coordinate is given by $R(-\alpha_{\mathrm{pol}})M_{\mathrm{pol}}R(\alpha_{\mathrm{pol}})$, in which R is the rotation matrix and M_{pol} is the Jones matrix of a polarizer set to pass p-polarized light:[44–46]

$$M_{\mathrm{pol}}(\alpha_{\mathrm{pol}}) = R(-\alpha_{\mathrm{pol}})M_{\mathrm{pol}}R(\alpha_{\mathrm{pol}}) = \begin{bmatrix} \cos^2\alpha_{\mathrm{pol}} & \sin\alpha_{\mathrm{pol}}\cos\alpha_{\mathrm{pol}} \\ \sin\alpha_{\mathrm{pol}}\cos\alpha_{\mathrm{pol}} & \sin^2\alpha_{\mathrm{pol}} \end{bmatrix}. \quad (7)$$

Analogous expressions can be derived for both half and quarter wave plates rotated by the angles α_Q and α_H, respectively,

$$M_Q(\alpha_Q) = R(-\alpha_Q)M_QR(\alpha_Q) = \begin{bmatrix} \cos 2\alpha_Q - i & \sin 2\alpha_Q \\ \sin 2\alpha_Q & -\cos 2\alpha_Q - i \end{bmatrix}, \quad (8)$$

$$M_H(\alpha_H) = R(-\alpha_H)M_HR(\alpha_H) = \begin{bmatrix} \cos 2\alpha_H & \sin 2\alpha_H \\ \sin 2\alpha_H & -\cos 2\alpha_H \end{bmatrix}. \quad (9)$$

1. Quarter-wave-plate–half-wave-plate–s polarizer [Fig. 1(a)]

The polarization state of the second harmonic light after passing the set of exigent optics can be evaluated by matrix multiplication of the frequency-doubled electric field generated at the sample[20]

$$\boldsymbol{e}^{2\omega}_{\mathrm{det}} = [M^{2\omega}_{\mathrm{pol}}(\pi/2)][M^{2\omega}_H(\alpha^{2\omega}_H)][M^{2\omega}_Q(\alpha^{2\omega}_Q)]\boldsymbol{e}^{2\omega}_{\mathrm{sample}}. \quad (10)$$

The vector $e^{2\omega}_{\mathrm{sample}}$ is the normalized Jones vector representing the polarization state of the frequency doubled light exiting the sample.[45,46] Substitution of the appropriate expressions for the Jones matrices for a quarter wave plate rotated an angle $\alpha^{2\omega}_Q$, a half wave plate rotated an angle $\alpha^{2\omega}_H$, and polarizer rotated 90°, followed by simplification using trigonometric identities allows Eq. (10) to be rewritten in the following form:

$$\boldsymbol{e}^{2\omega}_{\mathrm{det}} = \begin{bmatrix} e^{2\omega}_p \\ e^{2\omega}_s \end{bmatrix}_{\mathrm{det}} = \begin{bmatrix} 0 & 0 \\ \sin(2\alpha^{2\omega}_H - 2\alpha^{2\omega}_Q) - i\sin 2\alpha^{2\omega}_H & \cos(2\alpha^{2\omega}_H - 2\alpha^{2\omega}_Q) + i\cos 2\alpha^{2\omega}_H \end{bmatrix}\boldsymbol{e}^{2\omega}_{\mathrm{sample}}. \quad (11)$$

Using Eq. (11), the complete polarization state of the nonlinear beam can be obtained from the rotation angles $\alpha^{2\omega}_Q$ and $\alpha^{2\omega}_H$ that result in a minimum in the detected intensity (corresponding to the condition $|e^{2\omega}_{\mathrm{det}}|=0$). By analogy with linear ellipsometry, a complex-valued parameter ρ can be defined as the ratio of the p-polarized to s-polarized electric field components

$$\rho = \frac{e^{2\omega}_p}{e^{2\omega}_s} = \frac{\cos(2\alpha^{2\omega}_H - 2\alpha^{2\omega}_Q) + i\cos(2\alpha^{2\omega}_H)}{-\sin(2\alpha^{2\omega}_H - 2\alpha^{2\omega}_Q) + i\sin(2\alpha^{2\omega}_H)}. \quad (12)$$

The parameter ρ contains both amplitude and phase information. By analogy with linear ellipsometry, ellipsometric angles Ψ and Δ can be defined with respect to ρ:[46–48]

$$\tan\Psi = |\rho|, \quad (13)$$

$$\Delta = \arg(\rho). \quad (14)$$

In practice, it is often more convenient to simply use the complex parameter ρ in determination of the $\boldsymbol{\chi}^{(2)}$ tensor elements, rather than the angles Δ and Ψ.

2. Quarter-wave-plate–half-wave-plate–p polarizer [Fig. 1(b)]

The derivation of the expression for ρ in the case of p-polarized detection following a quarter-wave-plate–half-wave-plate combination is similar to that for s-polarized detection. Substitution of the appropriate Jones matrices followed by trigonometric simplification yields the following expression for the detected beam.

$$\mathbf{e}_{\mathrm{det}}^{2\omega}=\begin{bmatrix}\cos(2\alpha_H^{2\omega}-2\alpha_Q^{2\omega})-i\cos 2\alpha_H^{2\omega} & -\sin(2\alpha_H^{2\omega}-2\alpha_Q^{2\omega})-i\sin 2\alpha_H^{2\omega}\\ 0 & 0\end{bmatrix}\mathbf{e}_{\mathrm{sample}}^{2\omega}. \tag{15}$$

From the rotation angles $\alpha_Q^{2\omega}$ and $\alpha_H^{2\omega}$ that produce zero intensity at the detector, the complex parameter ρ can be easily obtained

$$\rho=\frac{e_p^{2\omega}}{e_s^{2\omega}}=\frac{\sin(2\alpha_H^{2\omega}-2\alpha_Q^{2\omega})+i\sin(2\alpha_H^{2\omega})}{\cos(2\alpha_H^{2\omega}-2\alpha_Q^{2\omega})-i\cos(2\alpha_H^{2\omega})}. \tag{16}$$

3. Quarter-wave-plate–rotating polarizer [Fig. 1(c)]

Null ellipsometry can also be achieved using only a quarter-wave plate and a polarizer. The resulting expression for ρ in terms of the quarter-wave plate rotation angle $\alpha_Q^{2\omega}$ and polarizer rotation angle $\alpha_{\mathrm{pol}}^{2\omega}$ producing an intensity minimum at the detector is given by

$$\rho=\frac{e_p^{2\omega}}{e_s^{2\omega}}=\frac{\sin(\alpha_{\mathrm{pol}}^{2\omega}-2\alpha_Q^{2\omega})+i\sin(\alpha_{\mathrm{pol}}^{2\omega})}{\cos(\alpha_{\mathrm{pol}}^{2\omega}-2\alpha_Q^{2\omega})-i\cos(\alpha_{\mathrm{pol}}^{2\omega})}. \tag{17}$$

The rotating polarizer null ellipsometry approach described by Eq. (17) and depicted in Fig. 1(c) has the advantage of requiring fewer optical components than the preceding configurations, but can potentially lead to undesirable artifacts if any subsequent optical elements exhibit polarization dependence (e.g., diffraction grating, side-on photomultiplier tubes, etc.).

4. Rotating analyzer ellipsometry (RAE) [Fig. 1(d)]

Determination of the complete polarization state of the nonlinear optical beam can be also determined using alternative ellipsometric methods. By analogy with approaches developed for linear ellipsometry, the polarization state can also be obtained from the detected intensity as a function of the rotation angle of a polarizer (analyzer), indicated in Fig. 1(d). Evaluation of the Jones matrices for a rotating analyzer configuration with the final polarizer set to pass *p*-polarized light follow closely the derivations presented in earlier work[46]

$$e_{\mathrm{det}}^{2\omega}(\alpha_{\mathrm{pol}}^{2\omega})=\begin{bmatrix}1 & 0\\ 0 & 0\end{bmatrix}\begin{bmatrix}\cos\alpha_{\mathrm{pol}}^{2\omega} & \sin\alpha_{\mathrm{pol}}^{2\omega}\\ -\sin\alpha_{\mathrm{pol}}^{2\omega} & \cos\alpha_{\mathrm{pol}}^{2\omega}\end{bmatrix}\begin{bmatrix}e_p^{2\omega}\\ e_s^{2\omega}\end{bmatrix}. \tag{18}$$

Evaluation of Eq. (18) yields the following general expression for the detected intensity:

$$I_{\mathrm{det}}^{2\omega}\propto|e_p^{2\omega}|^2\cos^2(\alpha_{\mathrm{pol}}^{2\omega})+|e_s^{2\omega}|^2\sin^2(\alpha_{\mathrm{pol}}^{2\omega})+2[\mathrm{Re}(e_p^{2\omega})\mathrm{Re}(e_s^{2\omega})+\mathrm{Im}(e_p^{2\omega})\mathrm{Im}(e_s^{2\omega})]\sin(\alpha_{\mathrm{pol}}^{2\omega})\cos(\alpha_{\mathrm{pol}}^{2\omega}). \tag{19}$$

Trigonometric substitution allows the above expression to be rewritten in the form

$$I_{\mathrm{det}}^{2\omega}\propto A\cos(2\alpha_{\mathrm{pol}}^{2\omega})+B\sin(2\alpha_{\mathrm{pol}}^{2\omega})+C, \tag{20a}$$

$$A=\tfrac{1}{2}(|e_p^{2\omega}|^2-|e_s^{2\omega}|^2), \tag{20b}$$

$$B=\mathrm{Re}[(e_p^{2\omega})(e_s^{2\omega})^*], \tag{20c}$$

$$C=\tfrac{1}{2}(|e_p^{2\omega}|^2+|e_s^{2\omega}|^2). \tag{20d}$$

Appropriate combinations of the three constants A, B, and C, then allow determination of the exigent polarization state:

$$|\rho|^2=\left(\frac{C+A}{C-A}\right), \tag{21a}$$

$$\mathrm{Re}(\rho)=\frac{B}{C-A}, \tag{21b}$$

$$\rho=\mathrm{Re}(\rho)+i\,\mathrm{Im}(\rho)=\frac{B\pm i\sqrt{C^2-A^2-B^2}}{C-A}. \tag{21c}$$

The sign ambiguity in ρ arises because the sense of ellipticity (right vs left) of the exigent beam cannot be determined *a priori* from simple rotating analyzer measurements. The analogous expressions for a polarizer designed to pass *s*-polarized light in Eq. (18) can be similarly derived:

$$|\rho|^2=\left(\frac{C-A}{C+A}\right), \tag{22a}$$

$$\mathrm{Re}(\rho)=\frac{-B}{C+A}, \tag{22b}$$

$$\rho=\mathrm{Re}(\rho)+i\,\mathrm{Im}(\rho)=\frac{-B\pm i\sqrt{C^2-A^2-B^2}}{C+A}. \tag{22c}$$

A closely related experimental setup to SHG-RAE is that of SHG using rotating half-wave plate ellipsometry (RHE). For this method, a rotating half wave plate is placed before a fixed polarizer as shown in Fig. 1(e). The mathematical treatment of the data is virtually identical to the SHG-RAE, except $\alpha_{\mathrm{pol}}^{2\omega}$ in Eq. (20a) is replaced with $2\alpha_H^{2\omega}$:

$$I_{\mathrm{det}}^{2\omega}\propto A\cos(4\alpha_H^{2\omega})+B\sin(4\alpha_H^{2\omega})+C. \tag{23}$$

All subsequent treatments are identical for both SHG-RHE and SHG-RAE.

The SHG-RHE experimental configuration has some practical advantages over the SHG-RAE. Photomultiplier tubes can routinely show differences in sensitivity depending on the polarization state of the light that is being detected, potentially leading to artifacts in subsequent fits of intensity-based measurements. The use of a rotating wave plate with a fixed polarizer ensures the same polarization is striking the PMT at all times. The SHG-RHE configuration also allows for the convenient use of two PMTs, providing two independent data sets in each experiment when using a polarizing beamsplitting cube or prism.

5. Rotating quarter-wave-plate ellipsometry (RQE)

The sign ambiguity arising in rotating analyzer ellipsometry can be resolved by using a rotating quarter-wave plate configuration. The Jones matrices for an optical path consisting of the sample, a rotating quarter-wave plate, and a fixed-polarizer set to pass p-polarized light prior to detection are given below [Fig. 1(e)]:

$$e_{\mathrm{det}}^{2\omega}(\alpha_Q^{2\omega}) = \begin{bmatrix} 1 & 0 \\ 0 & 0 \end{bmatrix} \begin{bmatrix} \cos(2\alpha_Q^{2\omega}) - i & \sin(2\alpha_Q^{2\omega}) \\ \sin(2\alpha_Q^{2\omega}) & -\cos(2\alpha_Q^{2\omega}) - i \end{bmatrix} \begin{bmatrix} e_p^{2\omega} \\ e_s^{2\omega} \end{bmatrix}. \tag{24}$$

Explicit evaluation of the detected intensity followed by substitution of appropriate trigonometric relations allows Eq. (24) to be reduced to the following form in a manner similar to that described for rotating polarizer ellipsometry:

$$I_{\mathrm{det}}^{2\omega} \propto K \sin(2\alpha_Q^{2\omega}) + L \sin(4\alpha_Q^{2\omega}) + M \cos(4\alpha_Q^{2\omega}) + N, \tag{25a}$$

$$K = 2\,\mathrm{Im}[(e_p^{2\omega})(e_s^{2\omega})^*], \tag{25b}$$

$$L = \mathrm{Re}[(e_p^{2\omega})(e_s^{2\omega})^*], \tag{25c}$$

$$M = \frac{1}{2}[|e_p^{2\omega}|^2 - |e_s^{2\omega}|^2], \tag{25d}$$

$$N = \frac{1}{2}[3|e_p^{2\omega}|^2 + |e_s^{2\omega}|^2]. \tag{25e}$$

Appropriate combinations of these relations yield the following expression for $\rho^{2\omega}$:

$$\rho = \frac{M+N}{2L - iK}. \tag{26}$$

If the detection geometry is changed such that the final fixed polarizer passes s-polarized light rather than p-polarized light, the expression for ρ changes to the following [Fig. 1(f)]:

$$\rho = \frac{-2L - iK}{M+N}. \tag{27}$$

B. Expressing the nonlinear optical polarization in terms of the $\chi^{(2)}$ tensor elements

Regardless of the specific optical configuration used (e.g., NONE, SHG-RAE, or SHG-RQE), the ellipsometry measurements yield the complex parameter ρ, which in turn describes the complete polarization state of the nonlinear optical beam. Projection of the incident and exigent s- and p-coordinate systems onto the surface (Cartesian) coordinate system leads to the following general expression for ρ in the case of SHG with a single incident beam (Fig. 2):[20,49]

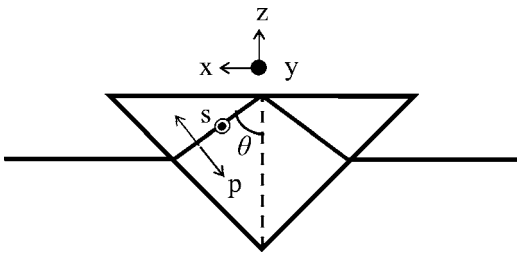

FIG. 2. Projection of the p- and s-polarization notation onto the Cartesian geometric system used to describe molecular orientation at the interface. The internal angle of incidence θ is 74.2°.

$$\rho = \frac{\chi_{ppp}(e_p^{\omega})^2 + 2\chi_{psp}e_s^{\omega}e_p^{\omega} + \chi_{pss}(e_s^{\omega})^2}{\chi_{spp}(e_p^{\omega})^2 + 2\chi_{ssp}e_s^{\omega}e_p^{\omega} + \chi_{sss}(e_s^{\omega})^2}. \tag{28}$$

The $\boldsymbol{\chi}^{(2)}$ tensor elements in Eq. (28) are model-independent parameters describing the macroscopic polarization characteristics of the sample.[49,50] In brief, the nonlinear optical response of the interfacial assembly is described by a $2\times2\times2$ Jones tensor relating the exigent Jones vector of the frequency-doubled beam to the two incident Jones vectors, which are identical in SHG [note: the definition of ρ in Eq. (28) differs from previous definitions[51] by the additional factor of 2 preceding χ_{psp} and χ_{ssp} arising from the formal use of a $2\times2\times2$ Jones tensor]. The phenomenological Jones tensor elements described in Eq. (28) can be obtained independently of the thin film model used to treat the interface.

The elements of the Jones tensors are complex functions of the angle of incidence, the optical constants of the media bridging the interface at all relevant wavelengths, the refractive indices and thickness of the SHG-active interfacial layer, and the nonlinear optical properties of the interface itself. Whereas the goals of traditional ellipsometry are generally to identify the thickness and/or refractive index of the interfacial layer from the elements of the Jones matrix describing the change in polarization state upon reflection (or transmission), the objectives of nonlinear optical ellipsometry measurements are to relate the elements of the rank three Jones tensor to the angle-independent surface tensor elements, which can in turn be related directly back to surface and molecular structure. In uniaxially oriented films, the relationship between the $2\times2\times2$ Jones tensor elements (which depend intimately on the angle of incidence) and the angle-independent $3\times3\times3$ Cartesian surface tensor elements described by Eq. (1) are given by the expressions[49]

$$\chi_{ppp} = \mp s_3\chi_{XXZ} + s_5\chi_{ZXX} + s_7\chi_{ZZZ}, \tag{29a}$$

$$\chi_{psp} = \mp \tfrac{1}{2}s_4\chi_{XYZ}, \tag{29b}$$

$$\chi_{pss} = s_6\chi_{ZYY}, \tag{29c}$$

$$\chi_{spp} = s_2\chi_{YXZ}, \tag{29d}$$

$$\chi_{ssp} = \tfrac{1}{2}s_1\chi_{YYZ}, \tag{29e}$$

$$\chi_{sss} = 0. \tag{29f}$$

The $\mp$ symbol should be positive for transmission measurements and negative for reflection and total internal reflection measurements. Virtually all of the information obtained using traditional ellipsometric approaches is contained within the Fresnel factors and geometric terms in the *s* coefficients. Explicit expressions for the *s* coefficients in Eq. (29) have been reported previously for measurements performed in reflection and total internal reflection.[49]

C. Experimental determination of the $\chi^{(2)}$ tensor elements

The set of optics used to prepare the polarization state of the incident beam can also be treated in a modular manner. In the following discussion, it will be assumed that the optical components preceding the sample consist of a fixed polarizer (or equivalently, a polarized laser source), a rotatable half wave plate, and a fixed quarter wave plate oriented at ±45°. The polarizer and the quarter wave plate may each be fixed at one of two settings (*s* or *p* and ±45°, respectively), providing four general cases for considering the incident optics. In general, the polarization of light that reaches the sample can be described by the expression

$$\boldsymbol{e}^{\omega} = M_Q M_H M_{\text{pol}} \boldsymbol{e}^{\omega}_{\text{in}}. \tag{30}$$

The four different combinations of the considered settings for the polarizer and the quarter-wave plate lead to only two unique outcomes for the polarization state of the beam entering the sample as a function of the half-wave plate rotation angle α_H^{ω} and are referred to as configurations A and B.

1. Configuration A

In configuration A, two different combinations (*pol* set to pass *s*-polarized with $Q=-45°$ [Fig. 3(a)] and *pol* set to pass *p*-polarized with $Q=45°$ [Fig. 3(b)]) yield identical incident electric fields as a function of α_H^{ω}. Substituting the appropriate Jones matrices and performing the matrix multiplication yields the following expression for the polarization of the light in terms of the rotation angle of the half-wave plate

$$\boldsymbol{e}^{\omega} = \frac{1}{\sqrt{2}} \begin{bmatrix} \exp(-i2\alpha_H^{\omega}) \\ i\exp(i2\alpha_H^{\omega}) \end{bmatrix}. \tag{31}$$

2. Configuration B

By analogy with configuration A, two different combinations (*pol* set to pass *s*-polarized with $Q=45°$ [Fig. 3(c)] and *pol* set to pass *p*-polarized with $Q=-45°$ [Fig. 3(d)]) yield identical incident electric fields

$$\boldsymbol{e}^{\omega}_{\text{sample}} = \frac{1}{\sqrt{2}} \begin{bmatrix} \exp(i2\alpha_H^{\omega}) \\ -i\exp(-i2\alpha_H^{\omega}) \end{bmatrix}. \tag{32}$$

D. Modular assembly of the complete optical path

The modular relations described in the previous sections can be combined for a given instrumental configuration to determine the complete suite of $\boldsymbol{\chi}^{(2)}$ tensor elements present in SHG. Combining the relations in Eq. (31) or (32) with Eq. (28) provides the fully complex-valued ρ parameter in terms of the $\boldsymbol{\chi}^{(2)}$ tensor elements and the rotation angle optics that define the polarization of the incident light.

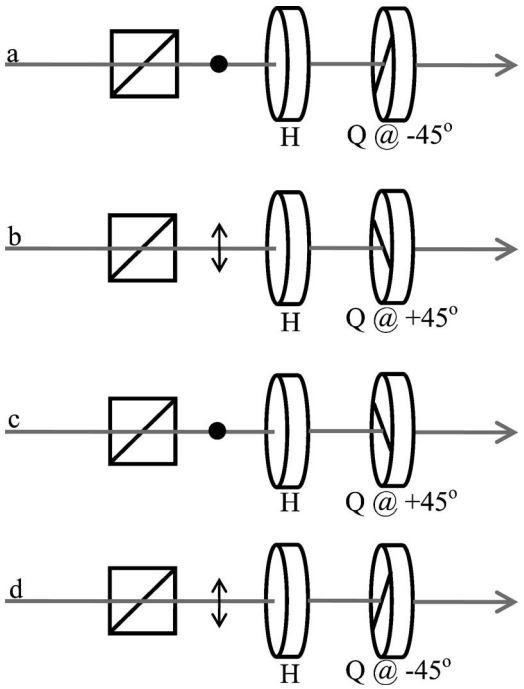

FIG. 3. Configurations for the incident optics (arrow represents the direction of the laser beam) where (a) polarizer set to pass *s*-polarizer light, rotating half-wave plate and quarter-wave plate at −45°; (b) polarizer set to pass *p*-polarizer light, rotating half-wave plate and quarter-wave plate at +45°; (c) polarizer set to pass *s*-polarizer light, rotating half-wave plate and quarter-wave plate at +45°; and (d) polarizer set to pass *p*-polarizer light, rotating half-wave plate and quarter-wave plate at −45°.

1. Case 1—Uniaxial chiral films using configuration A

In SHG measurements of uniaxially oriented films, substitution of the Jones vector for the optical field in Eq. (28) yields the following expression for ρ as a function of α_H^{ω}:

$$\rho(\alpha_H^{\omega}) = \frac{\chi_{ppp}\exp(-i4\alpha_H^{\omega}) + i2\chi_{psp} - \chi_{pss}\exp(i4\alpha_H^{\omega})}{\chi_{spp}\exp(-i4\alpha_H^{\omega}) + i2\chi_{ssp}}. \tag{33}$$

Evaluation of $\rho(\alpha_H^{\omega})$ for configuration A with $\alpha_H^{\omega}=-22.5°$, 0°, 22.5°, and 45° (corresponding to plane polarized with the polarization plane oriented +45°, right circularly polarized, plane polarized with the polarization plane oriented −45°, and left circularly polarized, respectively), results in the following set of expressions for the effective Jones tensor elements, derived in previous work:[50]

$$\frac{\chi_{spp}}{\chi_{ssp}} = 2\left[\frac{\Sigma_{R/L} - \Sigma_{+/-}}{i\Delta_{R/L} + \Delta_{+/-}}\right], \tag{34a}$$

$$\frac{\chi_{psp}}{\chi_{ssp}} = \frac{1}{2}\left[\Sigma_{+/-} + \frac{\chi_{spp}}{2\chi_{ssp}}\Delta_{+/-}\right], \tag{34b}$$

$$\frac{\chi_{pss}}{\chi_{ssp}} = \frac{1}{2}\left[(\Delta_{+/-} - i\Delta_{R/L}) + \frac{\chi_{spp}}{2\chi_{ssp}}(\Sigma_{+/-} - \Sigma_{R/L}) \right], \quad (34c)$$

$$\frac{\chi_{ppp}}{\chi_{ssp}} = \frac{1}{2}\left[(\Delta_{+/-} + i\Delta_{R/L}) + \frac{\chi_{spp}}{2\chi_{ssp}}(\Sigma_{+/-} + \Sigma_{R/L}) \right]. \quad (34d)$$

A shorthand notation has been introduced, in which $\Sigma_{+/-}=\rho(-22.5°)+\rho(22.5°)$, $\Sigma_{R/L}=\rho(0°)+\rho(45°)$, $\Delta_{+/-}=\rho(-22.5°)-\rho(22.5°)$, and $\Delta_{R/L}=\rho(0°)-\rho(45°)$. From experimental measurements of the ρ-values obtained for these four different incident polarization states, relative values of all five nonzero independent elements of the effective Jones $\boldsymbol{\chi}^{(2)}$ tensor can be uniquely obtained with full phase information.

2. Case 2—Uniaxial chiral films using configuration B

The expressions for the Jones $\boldsymbol{\chi}^{(2)}$ tensor elements in measurements acquired using configuration B are exactly identical to that for configuration A in Eq. (34) except $\rho(45°)$ now corresponds to right circularly polarized light and $\rho(0°)$ corresponds to left circularly polarized light [i.e., making the substitution $\Delta_{R/L}=\rho(45°)-\rho(0°)$ in Eq. (34)].

3. Case 3—Uniaxial achiral films using configuration A

In SHG measurements of uniaxial achiral films, the expressions in Eq. (34) simplify considerably. In the absence of chirality, $\rho(45°)=-\rho(0°)$ and $\rho(-22.5°)=-\rho(22.5°)$. Consequently, the set of complex-valued $\boldsymbol{\chi}^{(2)}$ tensor elements can be obtained from ellipsometry measurements performed from as few as just two incident polarization states (e.g., $\alpha_H^\omega=0°$ and $\alpha_H^\omega=22.5°$, corresponding to right circularly polarized light and linearly polarized light oriented at −45°, respectively):

$$\frac{\chi_{pss}}{\chi_{ssp}} = -\left[\rho(22.5^0) + i\rho(0^0)\right] = \frac{2s_6\chi_{ZXX}}{s_1\chi_{XXZ}}, \quad (35)$$

$$\frac{\chi_{ppp}}{\chi_{ssp}} = -\left[\rho(22.5^0) - i\rho(0^0)\right] = \frac{\mp 2s_3}{s_1} + \frac{2s_5\chi_{ZXX}}{s_1\chi_{XXZ}} + \frac{2s_7\chi_{ZZZ}}{s_1\chi_{XXZ}}, \quad (36)$$

4. Case 4—Uniaxial achiral films using configuration B

By analogy with case 3, simplification of Eq. (34) in the absence of chirality yields the following two compact relations, differing only from the expressions for configuration A in the sign of the $i\rho(0°)$ term:

$$\frac{\chi_{pss}}{\chi_{ssp}} = -\left[\rho(22.5^0) - i\rho(0^0)\right] = \frac{2s_6\chi_{ZXX}}{s_1\chi_{XXZ}}, \quad (37)$$

$$\frac{\chi_{ppp}}{\chi_{ssp}} = -\left[\rho(22.5^0) + i\rho(0^0)\right] = \frac{\mp 2s_3}{s_1} + \frac{2s_5\chi_{ZXX}}{s_1\chi_{XXZ}} + \frac{2s_7\chi_{ZZZ}}{s_1\chi_{XXZ}}. \quad (38)$$

E. Relationships between SHG-ORD, SHG-CD, SHG-LD, and nonlinear optical ellipsometry

Given that SHG-ORD experimental measurements are actually just rotating analyzer ellipsometry measurements acquired with a p-polarized incident beam, one would expect to find simplifying relationships connecting SHG-ORD with SHG-RAE and SHG-RHE. The general expression for SHG-RAE in Eq. (20a) differs from that given in Eq. (6), but the two expressions can be shown to be equivalent through the following substitutions:

$$A = \tfrac{1}{2}G\cos(2\phi), \quad (39a)$$

$$B = \tfrac{1}{2}G\sin(2\phi), \quad (39b)$$

$$C = F + \tfrac{1}{2}G. \quad (39c)$$

Correspondingly, the rotation angle of the primary polarization axis for a p-polarized fundamental beam ϕ_p is related to the Jones $\boldsymbol{\chi}^{(2)}$ tensor elements through the following expression:

$$\tan(2\phi_p) = \frac{B}{A} = \frac{2\,\mathrm{Re}(\chi_{ppp}\chi_{spp}{}^*)}{|\chi_{ppp}|^2 + |\chi_{spp}|^2}. \quad (40)$$

From inspection of Eqs. (4), (5), and (40), it is clear that precise knowledge of the complex-valued Jones tensor elements with phase information allows prediction of SHG-ORD as well as SHG-CD and SHG-LD, but the opposite is not necessarily true.

F. Molecular orientation information

In planar chromophores with pseudo-C_{2v} symmetry, excited states can be either B_1 like, in which $\beta_{x'x'z'}$ is the only symmetry allowed element of the molecular tensor, or A_1 like, in which $\beta_{z'z'z'}$ and $\beta_{z'x'x'}$ dominate the molecular response.[19] Explicit evaluation of Eq. (1) for a uniaxial surface system yields the following orientation average connecting the molecular nonlinearity to the nonlinear optical properties of the surface given by the $\boldsymbol{\chi}^{(2)}$ tensor in a planar chromophore of C_{2v} symmetry:[35,51,52]

$$\chi_{ZZZ} = N_s[\langle\cos^3\theta\rangle\beta_{z'z'z'} + \langle\sin^2\theta\cos\theta\cos^2\psi\rangle(\beta_{z'x'x'} + 2\beta_{x'x'z'})], \quad (41)$$

$$\chi_{ZXX} = \tfrac{1}{2}N_s[\langle\sin^2\theta\cos\theta\rangle\beta_{z'z'z'} + \langle\cos\theta\rangle\beta_{z'x'x'} - \langle\sin^2\theta\cos\theta\cos^2\psi\rangle(\beta_{z'x'x'} + 2\beta_{x'x'z'})], \quad (42)$$

$$\chi_{XXZ} = \tfrac{1}{2}N_s[\langle\sin^2\theta\cos\theta\rangle\beta_{z'z'z'} + \langle\cos\theta\rangle\beta_{x'x'z'} - \langle\sin^2\theta\cos\theta\cos^2\psi\rangle(\beta_{z'x'x'} + 2\beta_{x'x'z'})], \quad (43)$$

$$\chi_{XYZ} = \tfrac{1}{2}N_s[\langle\sin^2\theta\sin\psi\cos\psi\rangle(\beta_{x'x'z'} - \beta_{z'x'x'})]. \quad (44)$$

In Eqs. (41)–(44), N_s is the surface number density, θ is the tilt angle of the z' axis away from the surface normal, and ψ is the twist angle of the x' axis. In systems exhibiting a

random distribution in the twist angle ψ, an orientation parameter D can be defined by combination of the expressions in Eqs. (41)–(43).[53,54] For transitions to states of A_1-like symmetry in planar chromophores, the tensor elements $\beta_{z'z'z'}$ and $\beta_{z'x'x'}$ will dominate the molecular response,[19] leading to the following expression for the orientation parameter D:[54]

$$D = \frac{\langle \cos^3 \theta \rangle}{\langle \cos \theta \rangle} = \frac{\chi_{ZZZ} - \chi_{ZXX} + \chi_{XXZ}}{\chi_{ZZZ} - \chi_{ZXX} + 3\chi_{XXZ}}. \quad (45)$$

For transitions to states of B_1-like symmetry, only $\beta_{x'x'z'} = \beta_{x'z'x'}$ remain,[19] leading to the following expression for the orientation parameter D:

$$D = \frac{\langle \cos^3 \theta \rangle}{\langle \cos \theta \rangle} = \frac{\chi_{XXZ}}{\chi_{XXZ} - \chi_{ZXX}}. \quad (46)$$

From the orientation parameter D, an apparent orientation angle (θ^*) can be defined as the angle calculated if a δ-function orientation distribution in θ is assumed:

$$\theta^* = \arccos|D|^{1/2}. \quad (47)$$

It is worth emphasizing that the assumptions of a broad distribution in the twist angle ψ and a δ function distribution in θ should be used with caution. Experimental measurements of chiral and achiral systems have demonstrated that both approximations routinely fail in oriented thin surface films.[35,50,55,56]

G. Excited state information

The expression in Eq. (3) indicates that information related to the tensor for two-photon absorption (TPA) can be obtained from polarization analysis of SHG measurements. In the case of SHG resonant with A_1-like excited states, the ratio of the TPA tensor elements $R = \alpha_{x'x'}/\alpha_{z'z'}$ can be obtained directly from appropriate combinations of $\boldsymbol{\chi}^{(2)}$ tensor elements given in Eqs. (41)–(43)

$$R = \frac{2\chi_{ZXX} - 2\chi_{XXZ}}{\chi_{ZZZ} + 2\chi_{XXZ}} = \frac{\beta_{z'x'x'}}{\beta_{z'z'z'}} = \frac{\alpha_{x'x'}}{\alpha_{z'z'}}. \quad (48)$$

From Eq. (48), measurements of the ratio R yield information on the polarization-dependence of TPA.

III. EXPERIMENTAL SECTION

All experiments were performed on an instrument modified from one described in earlier work.[20] The optical pathway (Fig. 4) consisted of Nd:YAG laser source (New Wave Research Polaris, 1064 nm, 5–7 ns pulses, 20 Hz, ~1 mJ/pulse) followed by a half wave plate/Glan laser prism combination for attenuation of the fundamental beam. A computer-controlled rotating half-wave plate and fixed quarter-wave plate ($\alpha_Q^\omega = -45°$) controlled the incident polarization. A lens and visible blocking filter preceded the sample cell. An infrared absorbing filter and a collimating lens followed the sample cell. A polarizing beam splitting cube allowed separation and detection of both the *s*- and *p*-polarized components of the beam after passage through the wave plates. An infrared filter and a 532 nm interference filter preceded each photomultiplier tube (Burle 8850) for the detection of the second harmonic wavelength at 532 nm. The addition of the second detector allowed for the simultaneous monitoring of both polarization components separated at the polarizing beamsplitter.

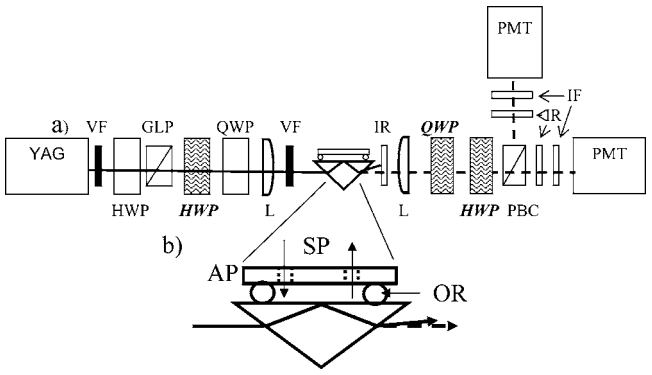

FIG. 4. (a) Schematic of the optical path for the instrument used in NONE. VF: visible absorbing filter; HWP: half-wave plate; GLP: Glan laser polarizer; QWP: quarter-wave plate; L: planoconvex lens; IR: infrared absorbing filter; PBC: polarizing beam splitting cube; IF: 532 nm interference filter. (b) Schematic of the total internal reflection flow cell. SP: sample inlet and outlet ports; AP: aluminum plate; OR: o ring.

NONE, SHG-RQE, SHG-RHE, and SHG-ORD measurements were performed for both fluorescein isothiocyanate labeled bovine serum albumin (FITC-BSA, Sigma) and rhodamine B labeled dextran, ~70 000 MW (RB-dex, Molecular Probes) surface layers. FITC-BSA interfaces were prepared by exposure of a cleaned fused silica prism surface to approximately 1 mg/mL FITC-BSA in a 0.01 M phosphate buffered saline (PBS) buffer using ultrapure water (Barnstead NANOpure system). RB-dex interfaces were generated by exposure to approximately 1 mg/mL RB-dex prepared in ultrapure water. In both systems, all measurements were performed with the prism in contact with the aqueous solutions.

SHG polarization measurements of model achiral interfaces were performed using dyes with absorbance maxima corresponding to on, near, and off resonance with the second harmonic of the beam. Solutions of 5.0×10^{-4} M Rhodamine 6G (R-6G, Aldrich, ~99% pure, $\lambda_{max} = 529.5$ nm, $\varepsilon_m = 110\,000$ cm^{-1} M^{-1}) in ultrapure water, 1.0×10^{-4} M disperse red 19 (DR-19, Aldrich, ~95% pure, $\lambda_{max} = 475.2$ nm, $\varepsilon_m = 27{,}000$ cm^{-1} M^{-1}) in 2-propanol (Mallinkrodt, HPLC grade), and 5.0×10^{-6} 1-docosyl-4-(4-hydroxystyryl)pyridinium bromide (DPB, Aldrich, $\lambda_{max} = 397.3$ nm, $\varepsilon_m = 27{,}000$ cm^{-1} M^{-1}; $\lambda_{max} = 574.0$ nm, $\varepsilon_m = 5{,}500$ cm^{-1} M^{-1}) in dichloromethane (Mallinkrodt, SpectraAR grade) were prepared. All measurements were performed in total internal reflection with the prism surface in direct contact with the solution. Measurements using dichloromethane were performed using a BK-7 glass prism to ensure total internal reflection.

Two different sample cells were used in the experiments. For the R-6G, DR-19, FITC-BSA, and RB-dex solutions, the

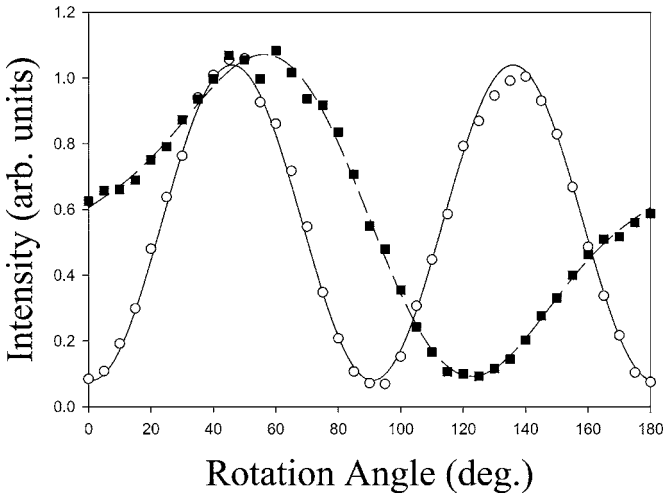

FIG. 5. Second harmonic plot of DR-19 fitted to Eqs. (49) and (50). The open circles represent the observed intensities while rotating the half wave plate with a fixed quarter-wave plate. The solid squares represent the rotating quarter-wave plate with a fixed half-wave plate. The lines represent the fitted data to the appropriate equations.

sample cell, consisting of a fused silica prism, a rubber o-ring, and a $\frac{1}{2}$-in square aluminum plate with an $\frac{1}{8}$-in hole, for sample addition/removal, held secure using mount clamps (1 in=2.54 cm). The volatility of the dichloromethane necessitated a closed sample chamber, constructed using a piece of aluminum $\left(1\text{ in}\times\frac{3}{4}\text{ in}\times\frac{1}{2}\text{ in}\right)$ containing a small sample well ($\frac{3}{8}$-in diameter and $\frac{1}{8}$-in depth) sealed to a BK-7 prism surface with a Teflon® o-ring.

Null angles were obtained using a LABVIEW® program written in house. The quarter and half wave plates along the detection pathway were positioned in computer controlled mounts (Newport SR50CC, with a Newport Universal Motion Controller/Driver). In a given NONE measurement, approximate values for the minimum angles were first determined by manual rotation of the wave plates as described previously.[20] Precise null angles were subsequently obtained by first recording the SHG intensity as a function of the quarter-wave plate rotation angle with the half-wave plate fixed and fitting the resulting response to the following general equation (Fig. 5):

$$I^{2\omega} = A\cos(4\alpha_H^{2\omega} + \delta_A) + B\cos(2\alpha_H^{2\omega} + \delta_B) + C. \quad (49)$$

The nonlinear curve fitting to Eq. (49) was used solely to identify the intnsity minima. The angle providing a minimum intensity of SH light was calculated from the Fourier coefficients A and B. The quarter-wave plate was then fixed at this minimum angle and the half-wave plate was rotated while mapping the intensity of the signal. The resulting curve was fit to Eq. (50) (the predicted response for a half wave plate), represented in Fig. 5

$$I^{2\omega} = A\cos(4\alpha_H^{2\omega} - \delta) + C. \quad (50)$$

The half-wave plate was fixed at the intensity minimum and the process was iteratively repeated until the values obtained for the null angles no longer changed significantly, a representative example of which is provided in Fig. 6. Reported errors are from 3–5 measurements.

SHG-RHE and SHG-RQE measurements were made using the same LABVIEW® software. For the SHG-RHE experiments, the second harmonic beam passed through a rotating half-wave plate and then through a fixed polarizer. The half-wave plate was rotated over 360° and the intensity of both s and p polarizations of light after the polarizer were measured using PMTs. The data acquired on the PMTs were both fit to Eq. (23). Parameters obtained from these fits were used to determine the respective ρ values. Errors were derived from the averages of 3–5 fits. For the SHG-RQE measurements, the second harmonic beam was passed through a rotating quarter wave plate and fixed polarizer. Both s and p polarizations were measured and fit to Eq. (25a). Errors were derived from the averages of 3–5 fits.

Molecular modeling calculations of DR-19, R-6G, and DPB were performed using GAUSSIAN 98.[57] Geometry optimization was performed using either restricted Hartree-Fock method with a STO-3G basis set (DPB and DR-19) or with the restricted B3LYP density functional theory method with the 6-31G basis set. Excited state calculations performed on the optimized structure were done with restricted ZINDO including the contributions from 100 excited states in determination of the TPA tensors. Consistent with previous modeling calculations,[58–61] the calculations for the TPA tensors (or equivalently, the hyperpolarizability tensors) for SHG

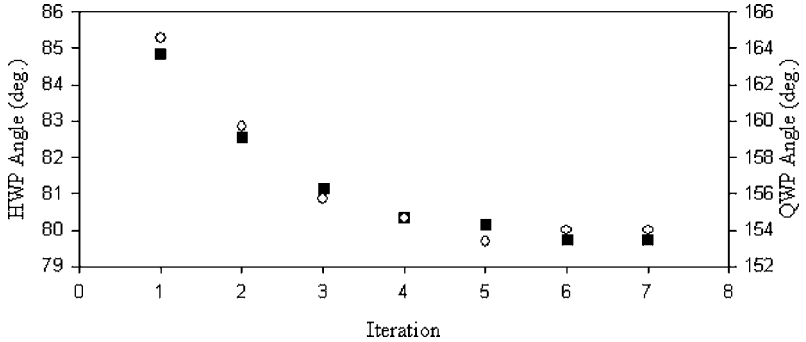

FIG. 6. Experimentally determined minimum angles for the iterative approach using automated NONE, the open circles represent the half wave plate angles and the solid squares represent the quarter-wave plate angles. The iterations converge to the reported null angles, which were determined to be 79.9° (±0.2°) and 153.8° (±0.5°) for the half- and quarter-wave plates, respectively.

TABLE I. Summary of null angles and determined ρ values.

	R-6G	DR-19	DPB
$\alpha_Q^\omega=0°$	[a]	129.2°(±0.7°)	−33.3°(±0.9°)
$\alpha_H^\omega=0°$	[a]	4.6°(±0.1°)	16.3°(±0.9°)
$\alpha_Q^\omega=22.5°$	112.8°(±0.5°)	153.8°(0.5°)	161.4.5°(±0.8°)
$\alpha_H^\omega=22.5°$	154.7°(±0.3°)	79.9°(±0.2°)	−2.5°(±0.3°)
ρ_0	0.00(±0.03)	0.55(±0.03)	0.48(±0.03)
	$-0.99i$(±0.03i)	$-0.963i$(±0.002i)	$-0.59i$(±0.04i)
$\rho_{22.5}$	−0.38(±0.02)	−1.92(±0.05)	−1.86(±0.07)
	$+0.345i$(±0.005i)	$-0.515i$(±0.002i)	$-1.57i$(±0.09i)

[a]The wave plate angles for R-6G did not converge for an incident polarization when $\alpha_H^\omega=0°$. The production of nearly perfectly circularly polarized light yields a number of angles that produce null values.

required summation of the contributions of the first ~100 excited states in order to obtain satisfactory convergence.

IV. RESULTS AND DISCUSSION

Values for the ellipsometric parameters ρ were obtained using several different nonlinear optical ellipsometric approaches and instrumental configurations. Table I contains the tabulated ρ values acquired using NONE for the resonant, near-resonant, and off-resonant achiral molecular systems, R-6G, DR-19, and DPB, respectively. Figures 7 and 8

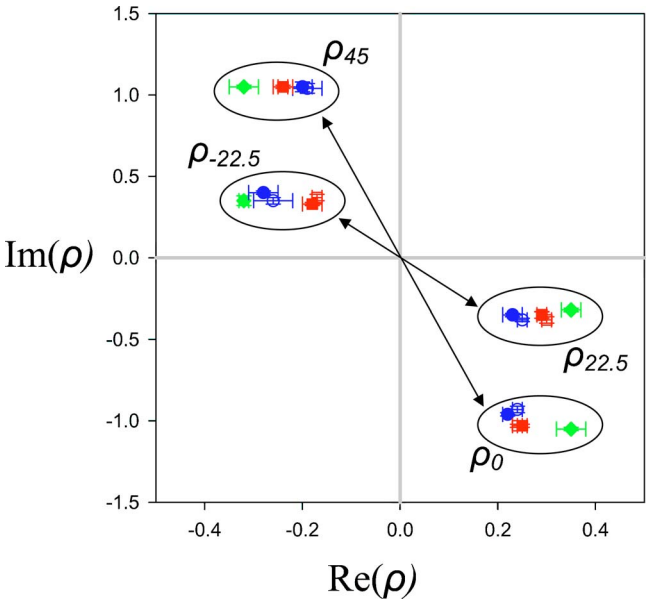

FIG. 7. (Color online) Extracted ρ values for rhodamine labeled dextran used to compare the polarization detection techniques where green diamonds represent NONE, red squares represent RHE, and blue circles represent RQE (for both RHE and RQE solid symbols are the values obtained from the *s*-detected fit and the open symbols are from the *p*-detected fit). Circled groups represent the ρ value obtained for the detection setups when using the same incident polarization (noted on the graph).

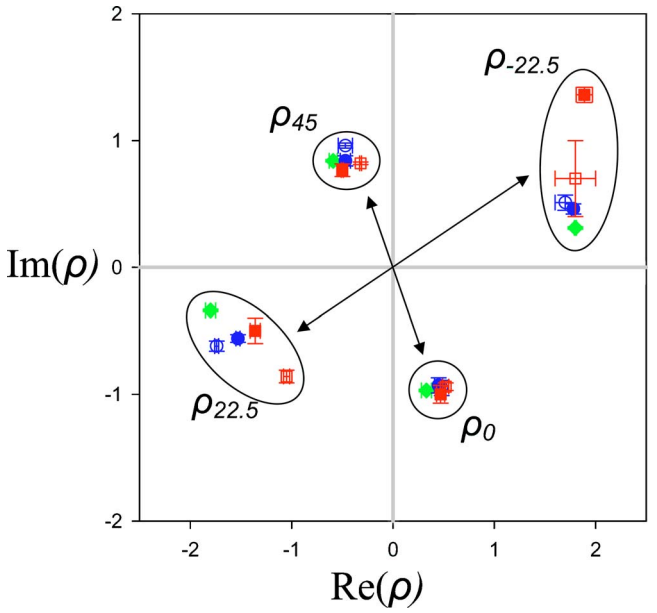

FIG. 8. (Color online) Extracted ρ values for FITC-BSA used to compare the the polarization detection techniques where green diamonds represent NONE, red squares represent RHE, and blue circles represent RQE (for both RHE and RQE solid symbols are the values obtained from the *s*-detected fit and the open symbols are from the *p*-detected fit). Circled groups represent the ρ value obtained for the detection setups when using the same incident polarization (noted on the graph).

contain a summary of the ρ values measured from two chiral surfaces (RB-dex and FITC-BSA, respectively) using three of the ellipsometric methods described in this work (full tables of these ρ values are available in the Supporting Information). In both the SHG-RQE and SHG-RHE measurements, the use of the instrument depicted in Fig. 4 allowed for the simultaneous acquisition of data using both configurations. As can be seen by inspection of Table I and Figs. 7 and 8, similar values for ρ were obtained for all of the different measurement approaches. It is worth noting that the values for ρ were outside of experimental error of each other in several instances, presumably resulting from the use of relatively small data sets (3 to 5 measurements for each data set), the possible presence of minor systematic errors, and/or computational complications associated with error propagation in complex numbers.

Analogous to knowledge of the wave functions in quantum mechanics, knowledge of the set of complex ρ values (two in SHG measurements of uniaxial achiral interfaces and four in chiral interfaces) allows for the prediction of the detected intensity expected for any combination of incident and exigent wave plates. Appropriate combinations of the ρ values yield the effective Jones $\chi^{(2)}$ tensor elements that describe the nonlinear optical susceptibility of the interfacial layer, retaining relative phase information [e.g., in Eq. (35)]. The Jones $\chi^{(2)}$ tensor elements are independent of the particular model used to relate the incident and exigent optical fields to the fields within the interfacial layer (i.e., the Fresnel factors). From these Jones tensor elements, the predicted intensities were calculated as a function of the exigent

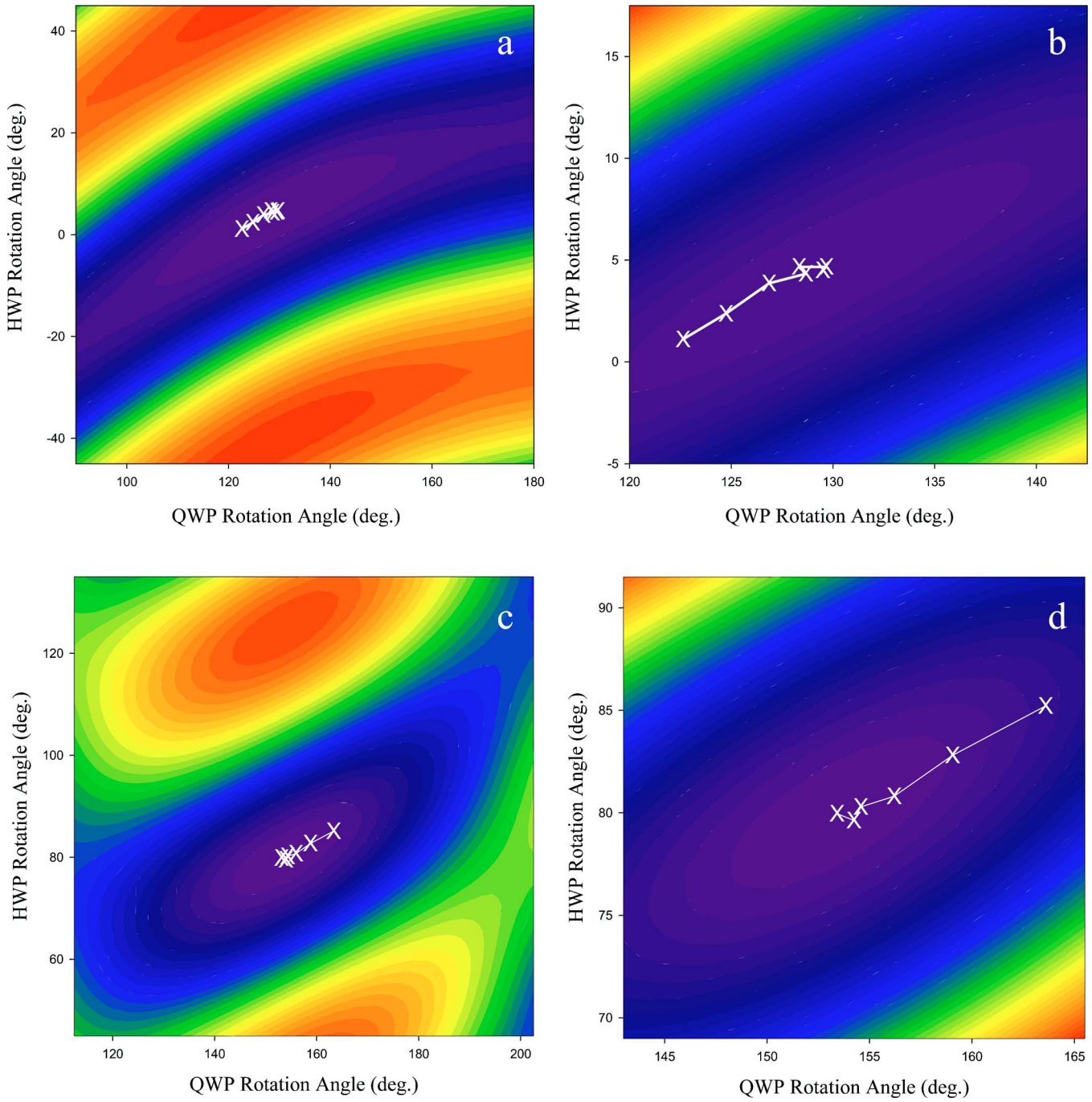

FIG. 9. (Color online) Predicted second harmonic intensity spectrum for DR-19 at the two incident polarizations used during the experiment (red represents the maximum intensity of arbitrary units and blue is the minimum intensity). The X's mark the null angle coordinates determined using automated NONE. The X's converge towards the minimum in the bowl shape of the intensity spectrum. (a) Represents an input polarization of $\alpha_H=0°$ and $\alpha_Q=-45°$, (b) is an expanded view of the region around the null angle, (c) has an input polarization of $\alpha_H=22.5°$ and $\alpha_Q=-45°$, (d) being the corresponding expanded region.

half wave plate and quarter wave plate rotation angles for a DR-19 monolayer film, shown in Figs. 9(a) and 9(b) for $\alpha_H=0°$ and in Figs. 9(c) and 9(d) for $\alpha_H=22.5°$. Superimposed on the calculated intensity "surfaces" are the experimental data demonstrating the iterative convergence to the intensity minima in the NONE measurements. The only information required to generate the full set of intensity surfaces shown in the figures (as well as for the construction of analogous plots for any different incident polarization state) was the locations of the two minima shown in the figure and highlighted in the expanded views. Analogous surfaces for the chiral systems can be constructed from the combined set of four ρ values.

In one particularly interesting case, the null angles for a silica surface in contact with the R-6G solution did not converge after multiple iterations with a right circularly polar-

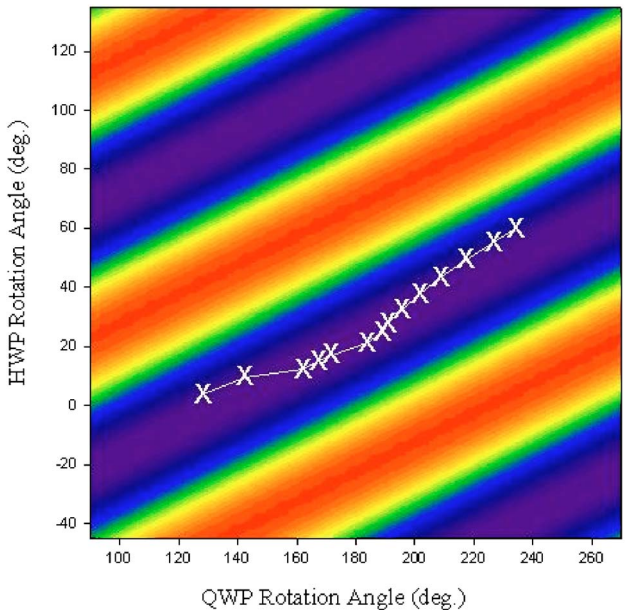

FIG. 10. (Color online) Predicted second harmonic intensity map for R-6G at an incident polarization of $\alpha_H=0°$ and $\alpha_Q=-45°$. This incident combination yielded light which possesses an intensity spectrum of a series of ridges and troughs which correspond to the production of nearly perfectly circularly polarized second harmonic light. The X's mark the null angle coordinates determined using automated NONE. Since an infinite combination of α_H and α_Q angles exist that will yield null values, the observed null angle combinations follow along the base of the trough, and do not converge to one set of angles.

ized incident beam (Fig. 10). This poor convergence can be understood by inspection of the parameters describing the polarization state of the frequency doubled beam. Under these conditions and for this sample, $\rho \cong 0-1i$ (Table I) indicating that the exigent light is almost perfectly circularly polarized. The projected intensity map of the second harmonic signal for this set of incident polarization conditions shown in Fig. 10 clarifies the reasons for the poor convergence. For purely circularly polarized light, any arbitrary rotation angle of the quarter wave plate generates purely linearly polarized light. Consequently, the global minimum of the intensity surface was so shallow that it could not be unambiguously identified within experimental error.

Combinations of the ρ values using Eqs. (35) and (36) together with the Fresnel factors evaluated using a thin film model developed previously[49] allowed for the determination of the $\chi^{(2)}$ tensor elements describing the resonant, near-resonant, and nonresonant achiral dye films, R-6G, DR-19, and DPB, respectively, which are compiled in Table II. Overall, the measured values are in good agreement with expectations based on symmetry analysis and quantum chemical calculations. For the resonant transition to the B_1 state in R-6G, the transition moment is oriented along the long axis (i.e., the x' axis) and perpendicular to the C_2 axis (i.e., the z' axis), in which case the $\beta_{x'x'z'}=\beta_{x'z'x'}$ are the only symmetry-allowed elements remaining in the molecular $\beta^{(2)}$ tensor. Under these conditions, the χ_{ZZZ}/χ_{ZXX} tensor ratio should be $\sim -2+0i$.[19,51,62] A value of $-1.81(\pm.02)-0.7i(\pm 0.1i)$ was obtained using NONE. Quantum chemical calculations for DR-19 and DPB performed in this work both indicated that the molecular tensors are dominated by the $\beta_{z'z'z'}$ element, in which the z' axis is the long axis of the chromophore. In this case, χ_{ZXX}/χ_{XXZ} tensor ratio is expected to be ~ 1.[19,51,62] NONE measurements yielded ratios of $1.00(\pm.04)-0.04i(\pm 0.04i)$ and $1.34(\pm 0.01)+1.1i(\pm 0.1i)$ for DR-19 and DPB, respectively. The results of the measurements for DR-19 and DPB are similar to those reported previously using a manually nulled instrument, although the automated system provided more precise measurements than those obtained in earlier work.[20]

A. Extraction of orientation information

The molecular orientation parameters D calculated for DR-19 and DPB [Eq. (45)] and for R-6G [Eq. (46)] are summarized in Table II. In the limit of a broad orientation distribution and for resonance enhancement with a single, spectrally resolved transition, a value of $D \cong 0.6+0i$ is expected.[55,63,64] All three dyes produced predominantly real orientation parameters approximately equal to 0.6. The apparent orientation angles for R-6G, DR-19, and DPB calculated from the values for D were be $38.5°(\pm 0.7°)$, $39.5°(\pm 0.9°)$, and $43°(\pm 2°)$, respectively, which are all within two standard deviations of the magic angle result of 39.2°, expected for a broad orientation distribution.[55,63,64] For physisorbed dye molecules assembled at solid-liquid interfaces, it is entirely reasonable to expect a broad distribu-

TABLE II. Summary of the surface $\boldsymbol{\chi}^{(2)}$ tensor elements and derived information.

	R-6G	DR-19	DPB
χ_{XXZ}	1	1	1
χ_{ZXX}	$-0.64(\pm 0.03)+0.37i(\pm 0.03i)$	$1.00(\pm 0.04)-0.04i(\pm 0.04i)$	$1.34(\pm 0.01)+1.1i(\pm 0.1i)$
χ_{ZZZ}	$1.42(\pm 0.01)-0.24i(\pm 0.04i)$	$2.74(\pm 0.05)+0.75i(\pm 0.01i)$	$2.43(\pm 0.07)+1.75i(\pm 0.09i)$
χ_{ZZZ}/χ_{ZXX}	$-1.81(\pm 0.02)-0.7i(\pm 0.1i)$	$2.72(\pm 0.02)+0.9i(\pm 0.1i)$	$1.7(\pm 0.1)-0.12i(\pm 0.08i)$
D	$0.61(\pm 0.01)-0.05i(\pm 0.01i)$	$0.59(\pm 0.01)+0.07i(\pm 0.01i)$	$0.52(\pm 0.02)+0.07i(\pm 0.04i)$
θ^a	$38.5°(\pm 0.7°)$	$39.5°(\pm 0.9°)$	$43°(\pm 2°)$
R_{exp}		$0.00(\pm 0.02)-0.02i(\pm 0.01i)$	$0.29(\pm .02)+0.21i(\pm 0.03i)$
R_{cal}		-0.02	-0.02

[a]All of the surface $\boldsymbol{\chi}^{(2)}$ tensor elements are normalized to χ_{XXZ}.

tion in surface orientation angles. Recovery of the magic angle result in resonant, near-resonant, and off-resonant dyes with significantly different symmetry properties and with no adjustable parameters supports the accuracy and reliability of the experimentally measured $\boldsymbol{\chi}^{(2)}$ tensor elements.

B. Excited state symmetry information

The measured $\boldsymbol{\chi}^{(2)}$ elements depend on both the molecular orientation and the molecular symmetry and provides a novel means of directly measuring the "depolarization ratio" of the TPA tensor. In the case of R-6G, the depolarization is relatively straightforward to evaluate by nature of the pseudo-C_{2v} symmetry. Since $\beta_{x'x'z'}=\beta_{x'z'x'}$ are the only remaining symmetry-allowed elements in the $\boldsymbol{\beta}^{(2)}$ tensor, $\alpha_{x'z'}$ and $\alpha_{z'x'}$ are the only nonzero elements in the TPA tensor. Diagonalizing this symmetric TPA tensor yields two equal and opposite principal elements, for which $R=-1$. In DR-19 and DPB, the TPA tensor contains symmetry-allowed contributions along the long axis, perpendicular to the long axis within the molecular plane, and orthogonal to the molecular plane. Quantum chemical calculations of the TPA tensors yielded R values of -0.02 for both DR-19 and DPB (with the negative sign indicating a sign change between $\alpha_{x'x'}$ and $\alpha_{z'z'}$). These values indicate strong TPA polarization along the long molecular axis (i.e., the z' axis) in each molecule, a relatively small short-axis (i.e., x' axis) contribution, and insignificant out-of-plane contributions. The measured depolarization ratios of the TPA tensors are consistent with these predictions of the modeling calculations, in which the R value for DR-19 was observed to be $0.00(\pm 0.02)-0.02i(\pm 0.01i)$ and the value for DPB was observed to be $0.29(\pm 0.02)+0.21i(\pm 0.03i)$. The value for DR-19 is within experimental error of the measured depolarization ratio, indicating that the two-photon transitions are predominantly polarized along the long z' axis (i.e., the pseudo-C_2 axis). The depolarization ratio does differ for DPB, however. The presence of a nonzero value for R with a significant imaginary contribution in the case of DPB may potentially be attributed to changes in the molecular tensor from aggregation at the interface.[65,66]

V. CONCLUSIONS

A modular ellipsometric approach was described for acquiring and interpreting polarization measurements in surface second harmonic measurements of ultrathin surface films. Consistent ρ values were obtained using multiple polarization analysis approaches, including null ellipsometry, rotating quarter wave plate ellipsometry, and rotating half-wave plate ellipsometry. NOE was demonstrated to be applicable off-resonance, near-resonance, and on-resonance. The extracted molecular orientation information corresponded well with expectations both with respect to molecular symmetry and the anticipated orientation distribution. For what we believe is the first time, the fully complex-valued $\boldsymbol{\chi}^{(2)}$ tensor elements were combined to directly yield a parameter directly related to the depolarization ratio of the molecular two-photon absorption tensor. The modular approach developed in this work supports a diverse array of experimental configuration in both SHG and SFG through a single, simple set of mathematical relations.

Note added. Supporting information: A link to an executable program for ellipsometric polarization analysis is available electronically.[67] Explicit tabulated values for the complex ρ values summarized in Figs. 7 and 8 are provided in the supporting information.[67]

ACKNOWLEDGMENTS

The authors gratefully acknowledge financial support from the NSF (Grant No. CHE0316177), the Research Corporation, the Beckman Young Investigator Program, the Camille and Henry Dreyfus Foundation, Eli Lilly, and Purdue University. We would also like to acknowledge the staff of the Jonathon Amy Facility for Chemical Instrumentation for providing insightful information. The authors would like to thank Charles Moad of the Scientific Data Analysis Lab of Indiana University for assistance in software development for data interpretation.

*Author to whom correspondence should be addressed.

[1] R. M. Corn and D. A. Higgins, Chem. Rev. (Washington, D.C.) **94**, 107 (1994).
[2] Y. R. Shen, Annu. Rev. Phys. Chem. **40**, 327 (1989).
[3] P. B. Miranda and Y. R. Shen, J. Phys. Chem. B **103**, 3292 (1999).
[4] C. D. Bain and P. R. Greene, Curr. Opin. Colloid Interface Sci. **6**, 313 (2001).
[5] M. J. Shultz, C. Schnitzer, D. Simonelli, and S. Baldelli, Int. Rev. Phys. Chem. **19**, 123 (2000).
[6] K. B. Eisenthal, Annu. Rev. Phys. Chem. **43**, 627 (1992).
[7] G. L. Richmond, Annu. Rev. Phys. Chem. **52**, 357 (2001).
[8] K. B. Eisenthal, Acc. Chem. Res. **26**, 636 (1993).
[9] K. B. Eisenthal, Chem. Rev. (Washington, D.C.) **96**, 1343 (1996).
[10] K. B. Eisenthal, J. Phys. Chem. **100**, 12997 (1996).
[11] Y. R. Shen, Nature (London) **337**, 519 (1989).
[12] V. Vogel, Curr. Opin. Colloid Interface Sci. **1**, 257 (1996).
[13] Y. R. Shen, Solid State Commun. **102**, 221 (1997).
[14] G. A. Somorjai and G. Rupprechter, J. Phys. Chem. B **103**, 1623 (1999).
[15] Y.-M. Chang, L. Xu, and H. W. K. Tom, Chem. Phys. **251**, 283 (2000).
[16] T. Rasing, Appl. Phys. A **59**, 531 (1994).
[17] D. H. Gracias, Z. Chen, Y. R. Shen, and G. A. Somorjai, Acc. Chem. Res. **32**, 930 (1999).
[18] C. Hirose, N. Akamatsu, and K. Domen, J. Chem. Phys. **96**, 997 (1992).
[19] A. J. Moad and G. J. Simpson, J. Phys. Chem. B **108**, 3548 (2004).
[20] R. M. Plocinik and G. J. Simpson, Anal. Chim. Acta **496**, 133

(2003).
[21] M. Kauranen, T. Verbiest, J. J. Maki, and A. Persoons, J. Chem. Phys. **101**, 8193 (1994).
[22] J. J. Maki, M. Kauranen, and A. Persoons, Phys. Rev. B **51**, 1425 (1995).
[23] T. Verbiest, M. Kauranen, A. Persoons, M. Ikonen, J. Kurkela, and H. Lemmetyinen, J. Am. Chem. Soc. **116**, 9203 (1994).
[24] M. Kauranen, T. Verbiest, and A. Persoons, J. Mod. Opt. **45**, 403 (1998).
[25] G. Wagnière, Chem. Phys. **54**, 411 (1981).
[26] G. Wagnière, J. Chem. Phys. **77**, 2786 (1982).
[27] J. J. Maki and A. Persoons, J. Chem. Phys. **104**, 9340 (1996).
[28] T. Verbiest, M. Kauranen, and A. Persoons, J. Mater. Chem. **9**, 2005 (1999).
[29] M. C. Schanne-Klein, F. Hache, T. Brotin, C. Andraud, and A. Collet, Chem. Phys. Lett. **338**, 159 (2001).
[30] S. v. Elshocht, T. Verbiest, M. Kauranen, A. Persoons, B. M. W. Langeveld-Voss, and E. W. Meijer, J. Chem. Phys. **107**, 8201 (1997).
[31] M. Kauranen, J. J. Maki, T. Verbiest, S. V. Elshocht, and A. Persoons, Phys. Rev. B **55**, R1985 (1997).
[32] F. Hache, S. K. Anderson, M. C. Schanne-Klein, and C. Flytzanis, Appl. Phys. B **68**, 321 (1999).
[33] F. Hache, H. Mesnil, and M. C. Schanne-Klein, J. Chem. Phys. **115**, 6707 (2001).
[34] M. C. Schanne-Klein, F. Hache, A. Roy, C. Flytzanis, and C. Payrastre, J. Chem. Phys. **108**, 9436 (1998).
[35] B. J. Burke, A. J. Moad, M. A. Polizzi, and G. J. Simpson, J. Am. Chem. Soc. **125**, 9111 (2003).
[36] T. Petralli-Mallow, T. M. Wong, J. D. Byers, H. I. Yee, and J. M. Hicks, J. Phys. Chem. **97**, 1383 (1993).
[37] J. D. Byers and J. M. Hicks, Chem. Phys. Lett. **231**, 216 (1994).
[38] J. D. Byers, H. I. Yee, and J. M. Hicks, J. Chem. Phys. **101**, 6233 (1994).
[39] Y. T. Lam and T. Thirunamachandran, J. Chem. Phys. **77**, 3810 (1982).
[40] J. J. Maki, T. Verbiest, M. Kauranen, S. V. Elshocht, and A. Persoons, J. Chem. Phys. **105**, 767 (1996).
[41] F. Hache, T. Boulesteix, M. C. Schanne-Klein, M. Alexandre, G. Lemercier, and C. Andraud, J. Phys. Chem. B **107**, 5261 (2003).
[42] L. Hecht and L. D. Barron, Mol. Phys. **89**, 61 (1996).
[43] V. Volkov, Y. P. Sviirko, V. F. Kamalov, L. Song, and M. A. El-Sayed, Biophys. J. **73**, 3164 (1997).
[44] R. Jones, J. Opt. Soc. Am. **31**, 488 (1941).
[45] B. E. A. Saleh and M. C. Teich, *Fundamentals of Photonics* (John Wiley and Sons, New York, 1991).
[46] R. M. A. Azzam and N. M. Bashara, *Ellipsometry and Polarized Light* (Elsevier, Amsterdam, 1987).
[47] A. J. Timson, R. D. Spencer-Smith, A. K. Alexander, R. Greef, and J. G. Frey, Meas. Sci. Technol. **14**, 508 (2003).
[48] A. J. Fordyce, W. J. Bullock, A. J. Timson, S. Haslam, R. D. Spencer-Smith, A. Alexander, and J. G. Frey, Mol. Phys. **99**, 677 (2001).
[49] G. J. Simpson, C. A. Dailey, R. Plocinik, A. J. Moad, M. A. Polizzi, and R. M. Everly, Anal. Chem. **77**, 215 (2005).
[50] M. A. Polizzi, R. M. Plocinik, and G. J. Simpson, J. Am. Chem. Soc. **126**, 5001 (2004).
[51] T. F. Heinz, in *Nonlinear Surface Electromagnetic Phenomena* (North-Holland, New York, 1991), p. 354.
[52] G. J. Simpson, ChemPhysChem **5**, 1301 (2004).
[53] G. J. Simpson, J. M. Perry, and C. L. Ashmore-Good, Phys. Rev. B **66**, 165437 (2002).
[54] D. A. Higgins, M. B. Abrams, S. K. Byerly, and R. M. Corn, Langmuir **8**, 1994 (1992).
[55] G. J. Simpson, S. Westerbuhr, and K. L. Rowlen, Anal. Chem. **72**, 887 (2000).
[56] G. J. Simpson and K. L. Rowlen, J. Am. Chem. Soc. **121**, 2635 (1999).
[57] M. J. Frisch *et al.*, GAUSSIAN 98 (Gaussian Inc., Pittsburgh, 1998).
[58] B. Champagne, P. Fischer, and A. D. Buckingham, Chem. Phys. Lett. **331**, 83 (2000).
[59] D. R. Kanis, M. A. Ratner, and T. J. Marks, Chem. Rev. (Washington, D.C.) **94**, 195 (1994).
[60] D. R. Kanis, M. A. Ratner, and T. J. Marks, J. Am. Chem. Soc. **114**, 10338 (1992).
[61] G. Hohlneicher and B. Dick, J. Chem. Phys. **70**, 5427 (1979).
[62] Y. R. Shen, *The Principles of Nonlinear Optics* (John Wiley & Sons, New York, 1984).
[63] G. J. Simpson, in *Chemistry* (University of Colorado, Boulder, CO, 2000), p. 406.
[64] G. J. Simpson and K. L. Rowlen, Acc. Chem. Res. **33**, 781 (2000).
[65] E. Stathatos and P. Lianos, Langmuir **13**, 259 (1997).
[66] S. Ma, Z. Lu, J. Song, L. Liu, W. Peng, J. Zhou, Z. Yu, W. Wang, and Z. Zhang, Langmuir **11**, 2751 (1995).
[67] See EPAPS Document No. E-PRBMDO-72-006532 for a supplementary program and tabulated values. This document can be reached via a direct link in the online article's HTML reference section or via the EPAPS homepage (http://www.aip.org/pubservs/epaps.html).